Available online at www.sciencedirect.com

Materials Chemistry and Physics 88 (2004) 97–101

MATERIALS CHEMISTRY AND PHYSICS

www.elsevier.com/locate/matchemphys

# Optical homogeneity and second harmonic generation in Li-rich Mg-doped $LiNbO_3$ crystals

Tao Zhang[a], Biao Wang[a,*], Ye-Quan Zhao[a], Shuang-Quan Fang[a], De-Cai Ma[a], Yu-Heng Xu[a,b]

[a] *Electro-Optics Technology Center, Harbin Institute of Technology, Harbin 150001, PR China*
[b] *Applied Chemistry Department, Harbin Institute of Technology, Harbin 150001, PR China*

Received 28 December 2003; received in revised form 19 February 2004; accepted 12 June 2004

## Abstract

A series of Mg-doped $LiNbO_3$ crystals were grown using Czochralski method with fixed 5 mol% Mg doping and a variety of Li/Nb ratio (Li/Nb = 0.946–1.08). From the UV–vis absorption spectra, it is found that the absorption edges of the off-congruent crystals successively shift to the violet band in comparison with that of congruent pure $LiNbO_3$. The birefringence gradient of these crystals was measured to investigate the optical homogeneity. In second harmonic generation (SHG) experiment, the SHG conversion efficiency was enhanced by the Mg doping and the increase of Li/Nb ratio. The dependences of the UV–vis absorption edges, the homogeneity and SHG properties on the Li concentration were explored. The results indicate that the crystal of Li/Nb = 1.02 is the most proper media for SHG application among the five crystals in the paper.

*Keywords:* Li-rich; Lithium niobate; Doping; Optical homogeneity; Second harmonic generation

## 1. Introduction

In the last decades lithium niobate (hereafter labeled $LiNbO_3$) crystal has gained great importance as a technological material. Its excellent electro-optical and nonlinear properties make it useful for optical switches, optical modulators, frequency doubling, and parametric oscillation [1–3]. However, all these applications need large single crystals with good optical homogeneity and strong optical damage resistance ability. It is reported that the optical damage, which is a serious problem when $LiNbO_3$ crystals are used for the above mentioned applications, can be noticeably reduced by increasing Li content [4,5] or doping damage-resistance impurities like Mg, Zn, In, and Sc [6–9]. On the other hand, the high doping level of impurities or Li excess subsequently increases the difficulty in growing high quality crystals with compositional-inhomogeneity-free. So optimizing $LiNbO_3$ with high damage resistance and testing homogeneity are an attractive work in the device application, especially, in second harmonic generation (SHG).

In this paper, Mg doping and Li-rich were employed to enhance the optical damage resistance ability. The optical homogeneity was characterized by birefringence gradient. The UV–vis absorption spectra and SHG properties (phase-matching temperature $T_{pm}$ and conversion efficiency $\eta$) of the Li-rich Mg-doped $LiNbO_3$ crystals were measured, respectively. On the basis of the experimental results, the dependences of the homogeneity and SHG properties on the Li concentration were explored.

## 2. Experimentals

### 2.1. Sample preparation

A series of $LiNbO_3$ crystals with fixed 5 mol% MgO doping and a variety of Li/Nb ratios were grown in

---

[*] Corresponding author. Tel.: +86 451 86418251; fax: +86 451 86418251.
*E-mail address:* tzhang_hit02@yahoo.com (B. Wang).

0254-0584/$ – see front matter © 2004 Elsevier B.V. All rights reserved.
doi:10.1016/j.matchemphys.2004.06.026

Table 1
Summary of doping level, Li/Nb ratio, and SHG properties for the $LiNbO_3$ crystals

| | Sample | | | | | |
|---|---|---|---|---|---|---|
| | No. 0 | No. 1 | No. 2 | No. 3 | No. 4 | No. 5 |
| Li/Nb starting composition (mol ratio) | 0.946 | 0.946 | 0.967 | 0.987 | 1.02 | 1.08 |
| MgO doping (mol%) | 0 | 5 | 5 | 5 | 5 | 5 |
| Li/Nb in crystal | 0.946 | 0.896 | 0.900 | 0.915 | 0.948 | 0.973 |
| MgO in crystal (mol%) | 0 | 4.60 | 4.45 | 4.38 | 4.26 | 4.01 |
| Crystal size (mm) | Ø35 × 40 | Ø35 × 35 | Ø30 × 35 | Ø30 × 35 | Ø30 × 30 | Ø30 × 30 |
| Wafer size (mm) | 10 × 2 × 10 | 10 × 2 × 10 | 10 × 2 × 10 | 10 × 2 × 10 | 10 × 2 × 10 | 10 × 2 × 10 |
| Treatment | As-grown | Oxidation | Oxidation | Oxidation | Oxidation | Oxidation |
| $\Delta R$ ($\times 10^{-5}$ cm$^{-1}$) | <0.3 | 1.1 | 1.5 | 2.0 | 4.8 | 10 |
| $T_{pm}$ (°C) | 0 | 112 | 115 | 112.3 | 108.4 | 106.5 |
| $\eta$ (%) | 10 | 24.7 | 28.2 | 32.9 | 37.4 | 18 |

an automatic diameter control (ADC) equipment using Czochralski method in air atmosphere, and a pure congruent $LiNbO_3$ crystal was also grown for comparison. The used raw materials, $Li_2CO_3$, $Nb_2O_5$ and MgO were all specpure (4N). The starting compositions are summarized in Table 1. In order to form polycrystalline bulk, the raw materials, which had been precisely weighed and thoroughly mixed for 12, were fully calcined at 700 °C for 2 h and then sintered at 1150 °C for 2 h. All crystals were pulled along the direction of [0 0 1] at a rate of 1.0–2.0 mm h$^{-1}$, and rotated at a rate of 15–20 rpm. About 30% of the initial charges were crystallized. The typical as-grown crystal size is approximately 30 mm in diameter and 30 mm in length.

The as-grown crystals were poled in a furnace where the temperature was hold at 1200 °C with an applied dc current density of 5 mA cm$^{-2}$ for 30 min. During the subsequent cool down period, the temperature decreased drastically from 1000 to 800 °C to avoid phase separation phenomenon. For optical characterization, the sample with the size of 10 mm × 2 mm × 10 mm ($a \times b \times c$) were cut along (0 1 0) plane from the middle of single-domain crystals. Some of the samples were buried into $Nb_2O_5$ powder to be reduced at 1140 °C for 10 h. The two opposite $y$-faces of all samples were ground by using SiC powder, and then polished to optical grade by using a 0.25 μm diamond solution for characterization (see Table 1).

### 2.2. Measurements

The non-polarized light UV–vis absorption spectra of Li-rich Mg-doped crystals were measured using a CARYIE-model UV–vis spectrophotometer with a wavelength between 300 and 600 nm at room temperature. For the concentration analysis, the upper parts of these crystals were used to determinate the Li, Nb and Mg contents by inductively coupled plasma (ICP) spectroscopy.

The optical homogeneity of the crystals was checked by means of birefringence gradient method. The experimental set-up and the corresponding vector diagram of the light polarization are shown in Fig. 1 and Fig. 2, respectively. A He–Ne laser of $\lambda$ = 633 nm was used as light source. The polarization directions of the polarizer and the analyzer were set along vector $\vec{P}$ and $\vec{A}$, respectively. The fast axis of the quarter-wave plate was perpendicular to $\vec{P}$. The crossing angle between the crystal optical axis ($c$-axis) and the vector $\vec{P}$ was 45°. The quarter-wave plate and the analyzer could be rotated in the range of $2\pi$. From Figs. 1 and 2, it could be obtained that after passing through the polarizer, the crystal and the quarter-wave plate in turn, the laser beam would become linearly polarized light, elliptically polarized light and linearly polarized light again, respectively. But the polarization direction of the transmitted light had been rotated some angle of $\varphi$. The birefringence gradient $\Delta R$ is described with the relation [10]

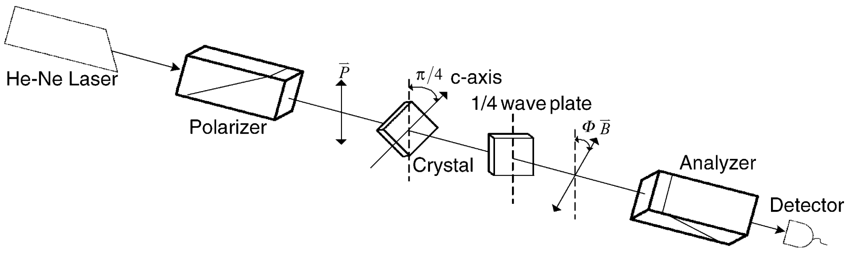

Fig. 1. Experimental set-up for birefringence gradient measurement. $\vec{P}$ and $\vec{B}$ are the polarization directions of the polarizer and the transmitted light through 1/4 wave plate, respectively.

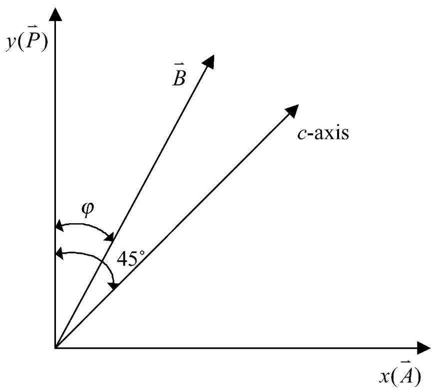

Fig. 2. Schematic drawing for the corresponding vectors in Fig. 1. (1) $\vec{A}$ is the polarization direction of the analyzer.

$$\Delta R = \frac{\partial(n_o - n_e)}{\partial l = \lambda(\varphi_2 - \varphi_1)/(\pi\, \Delta l d)}$$

where $n_o$ and $n_e$ are the ordinary and the extraordinary index, respectively, $\lambda$ is the wavelength of the laser beam in vacuum, $\Delta l$ is the distance between the measured two points, and $d$ is the crystal thickness. As shown in Fig. 2, the transmitted light intensity $I$ through the analyzer is

$$I = I_o \sin^2 \varphi$$

where $I_o$ is the incident intensity. So the birefringence gradient $\Delta R$ can be rewritten as

$$\Delta R = \frac{\lambda[\sin^{-1}(I_2/I_o)^{1/2} - \sin^{-1}(I_1/I_o)^{1/2}]}{\pi\, \Delta l d}$$

Since $LiNb_3$ crystal is uniaxially negative, the type of $o + o \to e$ phase matching was used to gain frequency-doubling light for testing the crystal SHG properties (phase-matching temperature $T_{pm}$ and conversion efficiency $\eta$). The experimental setup is shown in Fig. 3. A Q-switched Nd:YAG laser with an output wavelength of 1.06 μm and a pulse width of 11.5 ns was employed. The polarization vector of the ordinary beam was perpendicular to the crystal $c$-axis. The foreside and the backside planes of the samples were covered with 1.06 and 0.53 μm reflection reducing coatings, respectively, prior to being placed in a small heating furnace. The SHG light energy was measured by an energy detector. As the temperature increased, the output SHG energy $P_w$ changed as a function of the temperature $T$. When $P_w$ reached the maximum, the corresponding temperature was defined as the phase-matching temperature $T_{pm}$. The definition of conversation efficiency $\eta$ was the ratio of the maximal SHG energy to the basal wave energy.

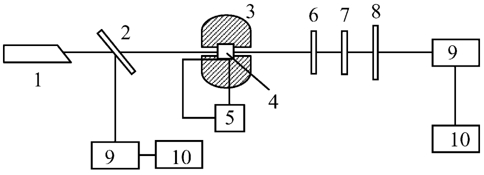

Fig. 3. Experimental set-up for SHG measurement. (1) Nd:YAG laser; (2) beam splitter; (3) heater; (4) sample; (5) temperature controller; (6) 1.06 μm reflective mirror; (7) green glass; (8) 0.53 μm interference light filter; (9) energy detector; (10) galvanometer.

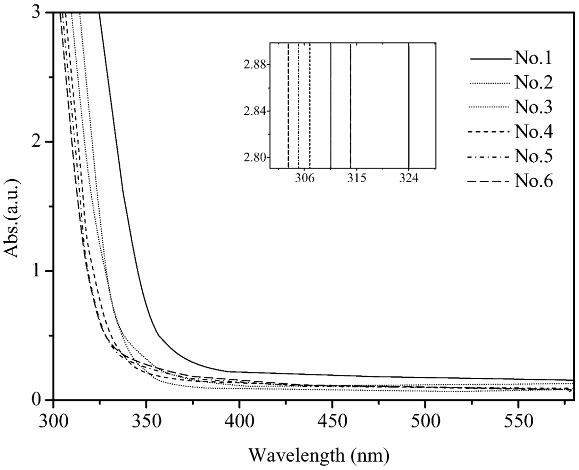

Fig. 4. Absorption spectra in the near ultraviolet and visible regions of the Li-rich Mg doped $LiNbO_3$ crystals.

## 3. Results and discussion

The UV–vis absorption spectra of these crystals are illustrated in Fig. 4. As shown in Fig. 4, the absorption edges of Li-rich Mg-doped crystals all shift to the violet band compared with that of pure $LiNbO_3$. Meanwhile, the levels of the violet shift are different with the increase of Li/Nb ratio. The absorption edge positions of the three crystals with Li/Nb = 0.987–1.08 are so close that it is difficult to distinguish them. The inset clearly shows the absorption edge positions. It has been known that the absorption edge position is related to the doping ions. In terms of the polarization theory introduced by Zhen et al. [11], it is suggested that Mg ions preferentialy replace the $Nb_{Li}$ defects in the crystal until the Mg doping concentration is over the threshold (>4.6 mol%). Since the polarization ability of Mg is much lower than that of Nb, the absorption edge position of Mg:$LiNbO_3$ (No. 2) crystal is markedly reduced from 324 to 314 nm compared with that of the pure $LiNbO_3$ (No. 1). As the Li/Nb ratio in the crystal increases (see Table 1), contrary to the $Nb_{Li}$ defects decreasing, the number of Li–O bond in oxygen octahedron will increase. So the absorption edges of the Li-rich Mg-doped $LiNbO_3$ crystals (Nos. 3–6) go on a shift to the violet band due to the polarization ability of Li ions lower than that of Nb ions.

Table 1 lists the birefringence gradient of the crystals. It is shown that the birefringence gradient $\Delta R$ increases with the increase of Li/Nb ratio. When Li/Nb ratio reaches 1.08, $\Delta R$ of the No. 5 crystal increases by a factor of 33 in comparison with that of pure $LiNbO_3$ (No. 0).

It is well known that the solid-liquid curve of the $Li_2O$–$Nb_2O_5$ phase diagram shows a congruent point around 48.6 mol% $Li_2O$ [12,13]. Depending on the control of stoichiometry in the melt, the Li concentration in the crystal may vary from boule to boule and even within a boule. As the Li/Nb ratio in the melt increases, the bigger extent of deviation from the congruent point will leads to Li compositional inhomogeneity in the crystal. In addition, the less intrinsic defects in the crystal with increase of Li/Nb ratio will make it more difficult for Mg entering the $LiNbO_3$ lattice at the same doping level (see Table 1), and therefore the distribution coefficient of Mg during crystal growth will change. This will cause the Mg ions' uniform distribution. As shown in Table 1, the birefringence gradients of Nos. 1–4 crystals have the same order of $10^{-5}$ $cm^{-1}$ though their melt compositions deviate from the congruent point. While in the case of No.5 crystal, the above-mentioned reasons are the most likely responsible for the bigger birefringence gradient. Moreover it must be referred that phase separation will also possibly lead to the bigger birefringence gradient occurrence in the highly Mg-doped (5 mol%) and Li-rich (Li/Nb = 1.08) $LiNbO_3$ crystal, although we have adopted some steps to avoid phase separation during the crystal annealing treatment.

The SHG properties ($\eta$, $T_{pm}$) of the crystals are shown in Table 1. With increasing Li/Nb ratio, the conversion efficiency $\eta$ rises up to 37.4% (Nos. 0–4), and then drops to 18% (No. 5). In nonstoichimetric $LiNbO_3$ crystals, there exist a large amount of defects, such as anti-site Nb ($Nb_{Li}$) and Li vacancies [14,15]. So far, some researchers [16,17] have pointed out that optical damage resistance increases as the Li vacancies increase. The increase in Li vacancies will make the photoconductivity higher, which may lead to the higher optical-damage resistance. On the basal of the above-mentioned opinions and UV–vis absorption spectra analysis, it is concluded that in Li-rich Mg-doped $LiNbO_3$ crystals Mg ions take priority of replacing anti-site Nb ($Nb_{Li}$), and then the other Mg ions occupy normal Li sites forming ${Mg_{Li}}^+$ defects. With the increase of Li/Nb ratio, the lattice will become more perfect and the $Nb_{Li}$ defects will become less and less in the crystal, so it means that more Mg ions enter Li sites and form ${Mg_{Li}}^+$. For the sake of charge compensation, it is required more Li vacancies (${V_{Li}}^-$) to generate. Since the total concentration of ${V_{Li}}^-$ increase in Li-rich crystals, the optical damage resistance and therefore the SHG efficiency are enhanced gradually (Nos. 0–4). However, for No. 5 crystal the low SHG efficiency is chiefly attributed to the worse optical quality.

Moreover, there is another probable reason to explain the SHG efficiency increase. In all $LiNbO_3$ crystals, even grown form rather pure melts, Fe of trace impurity are always present. $Fe^{2+/3+}$ ions as photorefractive centers usually occupy normal Li sites [18,19]. When Mg ions enter the crystal lattices, they replace $Nb_{Li}$ firstly, and then the additional Mg ions occupy Li sites. At the same time, $Fe^{2+/3+}$ ions on the Li sites will be repelled by Mg ions to Nb sites. If Li/Nb ratio goes up, most of the $Fe^{3+}$ ions will occupy Nb sites and lose their electron acceptor properties, which will lead to an increase in photoconductivity. Therefore, the photoconductivity increase is mainly responsible for the increase in SHG efficiency of the Li-rich Mg-doped $LiNbO_3$ crystals (Nos. 0–4).

## 4. Conclusions

A series of Li-rich Mg-doped $LiNbO_3$ crystals had been grown using the Czochralski method. The experimental results reveal that absorption edges shift to the violet, the birefringence gradient and the SHG conversion efficiency rise with the increase of Li/Nb ratio. According to the UV–vis absorption spectra, it is suggested that the difference of the polarization abilities between Mg, Li and Nb ions causes the violet shift of the absorption edges. The birefringence gradient increase is the result of compositional inhomogeneity. While for the SHG conversion efficiency, it is assumed that the increase of Li vacancies or $Fe^{3+}$ losing their electron acceptor properties results in the photoconductivity increase and therefore the SHG efficiency increase. Among the six crystals, the crystal of Li/Nb = 1.02 is the most proper media for SHG application.

## Acknowledgements

This work is financially supported by the National Research for Fundamental Key Projects No. 973 (G19990330), the National Advanced Technology Program No. 863 (2001AA31304), the National Natural Science Foundation (10172030), and the Nature Science Foundation of Heilongjiang Province (A01-01), People's Republic of China.

## References

[1] J.K. Yamamoto, T. Yamazaki, K. Yamaishi, Appl. Phys. Lett. 64 (24) (1994) 3228.
[2] L.E. Myers, G.D. Miller, R.C. Eckardt, M.M. Fejer, R.L. Byer, W.R. Bosenberg, Opt. Lett. 20 (1995) 52.
[3] Y. Furukawa, K. Kitamura, S. Takekawa, K. Niwa, Y. Yajima, N. Iyi, I. Mnushkina, P. Gunggenheim, J.M. Martin, J. Cryst. Growth 211 (2000) 230.
[4] M.H. Li, Y.H. Xu, R. Wang, X.H. Zhen, C.Z. Zhao, Cryst. Res. Technol. 36 (2001) 191.
[5] X.H. Zhen, W.S. Xu, C.Z. Zhao, L.C. Zhao, Y.H. Xu, Cryst. Res. Technol. 37 (2002) 976.
[6] G.G. Zhong, J. Jian, Z.K. Wu, Proceedings of the 11th International Quantum Electronics Conference, IEEE Cat. No. 80, CH 61-0, June 1980, p. 631.
[7] T.R. Volk, V.I. Pryalkin, N.M. Rubinina, Opt. Lett. 15 (18) (1990) 996.
[8] T.R. Volk, N.M. Rubinina, Ferroelect. Lett. 14 (1992) 37.
[9] J.K. Yamanoto, K. Kitamura, N. Iyi, S. Kimura, Y. Furukawa, M. Sato, Appl. Phys. Lett. 61 (1992) 2156.
[10] A.Z. Han, Y.K. Gao, S.W. Su, Chin. J. Synth. Cryst. 24 (2) (1995) 160 (in Chinese).
[11] X.H. Zhen, L.C. Zhao, Y.H. Xu, Appl. Phys. B 76 (2003) 655.

[12] R.L. Byer, J.F. Young, R.S. Feigelson, J. Appl. Phys. 41 (1970) 2320.

[13] J.R. Carruthers, G.L. Peterson, M. Grasso, P.M. Bridenbaugh, J. Appl. Phys. 42 (1971) 1846.

[14] N. Iyi, K. Kitamura, F. Izumi, J.K. Yamamoto, T. Hayashi, H. Asano, S. Kimura, J. Solid State Chem. 101 (1992) 340.

[15] N. Iyi, K. Kitamura, Y. Yajima, S. Kimura, J. Solid State Chem. 118 (1995) 118.

[16] N.B. Anghert, V.A. Pashkov, N.M. Solov'yeva, Zh. Eksp. Teor. Fiz. 26 (1972) 1666.

[17] Y. Furukawa, M. Sato, K. Kitamura, Y. Yajima, M. Minakata, J. Appl. Phys. 72 (1992) 3250.

[18] C. Prieto, C. Zaldo, Solid State Commun. 83 (1992) 819.

[19] J.J. Liu, W.L. Zhang, G.Y. Zhang, Solid State Commun. 98 (1996) 523.